Atomic-scale topography of rutile TiO2(110) in aqueous solutions: A study involving frequency-modulation atomic force microscopy

Xue, Shengkai
Sasahara,Akira
Onishi,Hiroshi

(Citation)
Journal of Chemical Physics,152(5):054703-054703

(Issue Date)
2020-02-07

(Resource Type)
journal article

(Version)
Accepted Manuscript

The Journal of Chemical Physics

Atomic-scale topography of rutile TiO_2(110) in aqueous solutions: a study involving frequency-modulation atomic force microscopy

Shengkai Xue, Akira Sasahara, and Hiroshi Onishi*

Department of Chemistry, School of Science, Kobe University, Rokko-dai, Nada, Kobe, Hyogo 657-8501, Japan

corresponding author's email address: oni@kobe-u.ac.jp

The interfaces between metal oxides and liquids represent the next frontier in the study of oxide chemistry. In this work, (110)-oriented rutile TiO_2 wafers were annealed in oxidative atmospheres and immersed in aqueous KCl solutions of pH 3, 6, and 11. Topographic imaging of the TiO_2 wafers was carried out in solution via atomic force microscopy using the frequency-modulation force detection technique. Crystalline terraces of 100 nm in width were observed with no sign of solution-induced etching. In a pH-6 solution, ridges parallel to the [001] axis with trenches in between were observed and assigned to the rows of oxygen anions protruding from the surface plane to the solution. Individual anions were further resolved in the ridges, revealing atomic-size protrusions located on the (1×1) meshes of the (110) truncation. The topography in an acidic solution (pH 3) was similar to that observed in a neutral solution and could be interpreted as protruding oxygen anions covered partially by protons. In a basic solution with pH 11, qualitatively different features were observed; atomic-size swellings formed a p(2×1) superstructure covering the surface, which was hypothesized to be Ti-OH^- on five-fold coordinated Ti cations in the surface plane. These results show the feasibility of advanced atomic force microscopy for probing metal-oxide surfaces submerged in liquids.

I. INTRODUCTION

The (110)-oriented rutile TiO_2 is a prototypical metal oxide used in surface science. Various atoms and molecules have been adsorbed on (110)-oriented wafers placed in a vacuum,[1] and a vacuum environment or one with a controlled amount of vapor provides the most convenient conditions for preparing and characterizing

well-defined surfaces with adsorbed chemical species. In recent years, liquid–TiO_2(110) interfaces have been investigated to compare the (110)-oriented rutile TiO_2 submerged in liquid with one isolated in a vacuum environment. However, experimental methods that are based on electrons or ions are generally not feasible for interfaces in a liquid. Instead, functional methods must be selected and optimized to provide reliable data, as outlined in a recent perspective.[2]

In the present study, topographic imaging of TiO_2(110) in water was investigated and optimized. Frequency-modulation atomic force microscopy (FM-AFM) was carried out on wafers annealed in oxidative atmospheres and immersed in aqueous KCl solutions with different pH values. This scanning probe method was developed originally for high-resolution imaging in vacuum; in the initial studies 25 years ago, individual atoms and atomic vacancies were visualized on Si[3,4] and InP[5] wafers placed in a vacuum. Oxygen anion vacancies on TiO_2(110) were subsequently observed in N_2 gas at atmospheric pressure.[6] Following the development of liquid-compatible microscopy,[7] a number of solids have been scanned in water and topographic images with atomic-scale resolution have been obtained. The application of this technique to metal oxides was reported for mica,[8,9] sapphire,[10] clay and aluminosilicate minerals,[11–13] $SrTiO_3$,[14] and brookite TiO_2.[15] One study resolved ridges and trenches, but not individual atoms, parallel to the [001] axis on TiO_2(110) immersed in pure water.[16]

The stoichiometric (110) truncation involves four atomic species when prepared in a vacuum. Five-fold coordinated and six-fold coordinated Ti^{4+} cations are located on a surface plane perpendicular to the [110] direction together with three-fold coordinated O^{2-} anions. Two-fold coordinated oxygen anions protrude from the plane by bridging two six-fold coordinated Ti cations, as illustrated in Fig. 1. When a probing tip traces the physical topography of the surface, as realized during FM-AFM imaging in a vacuum,[17,18] the bridging oxygen anions present ridges parallel to the [001] axis separated by trenches with five-fold coordinated Ti cations at the bottom.

The chemical composition of the (110) truncation can be complicated when immersed in aqueous solutions. Water is the primary component of the solution and can modify the surface. The five-fold coordinated Ti cations provide surface sites for molecular adsorption of water with its oxygen end down. The resultant Ti-OH_2 species are capable of deprotonation in a basic environment to produce Ti-OH^-. Simulations based on a multi-site complexation (MUSIC) model[19] and density functional theory[20] predicted the pKa of the reaction Ti-OH_2 ⇄ Ti-OH^- + H^+ to be 4.8 and 9, respectively. By contrast, the bridging oxygen anions are protonated in an acidic

solution. The pKa of the protonation–deprotonation equilibrium, Ti-OH^+-Ti ⇄ Ti-O-Ti + H^+, was estimated to be 2.8 in the MUSIC simulation.[19] The isoelectric point (i.e., the point of zero charge) has been determined experimentally on (110)-oriented wafers to be in a pH range of 4.8±0.3[19] or 4.8–5.5.[21]

Insert Fig. 1 here

FIG. 1. Stoichiometric (1×1) truncation of rutile (110) surface prepared in vacuum. The dark and white filled spheres represent Ti and O ions, respectively. Six-fold coordinated Ti cations are included in the bulk and are invisible in the drawing. The dashed lines mark a rectangular surface unit cell of 0.65 nm × 0.30 nm.

II. EXPERIMENTAL DETAILS

A. Wafer preparation

A mirror-polished 10 mm × 10 mm square (110)-oriented wafer of rutile TiO_2 (Shinkosha, STEP type) with a thickness of 0.5 mm was annealed in a two-step procedure using a tube furnace, as detailed in our earlier report.[22] Isolating the wafer from SiO_2-containing devices heated at 1000°C or higher temperatures was required to avoid Si contamination on the surface of the annealed wafer. The wafer was first heated at 1000°C for 12 h in a sapphire tube open to ambient air. Annealing at elevated temperature was effective for the formation of wide (110) terraces. Next, the wafer was further annealed at 500°C in a quartz tube filled with dry air, which was a mixture of O_2 and N_2 with a pressure ratio of 1:4. The moisture-free environment was efficient to provide the well-ordered TiO_2(110) surface.[22] Making the heated sapphire tube airtight was difficult, therefore a quartz tube was used for the second step. X-ray photoelectron spectroscopy was used to confirm that the wafer surface finished in the quartz tube was almost free from Si contamination, as shown in Fig. S1 in the supplementary material.

B. Topographic imaging in solutions

An annealed TiO_2 wafer was fixed on a fluorocarbon polymer disk. A droplet of imaging liquid [aqueous KCl solution (0.1 mol/L)] was placed on the wafer to avoid contact with the disk; any potential contamination on the disk surface would not be transferred to the wafer surface through the liquid. The cantilever was placed on top of the droplet and covered with a glass slip (Matsunami Glass). Prior to assembling, the slip was irradiated

with a Hg–Xe lamp (San-ei Electric, UVS-204S) for 90 min in air to remove possible organic contamination from the surface. The imaging solution of pH 6 was prepared using KCl (Nacalai tesque, 99.9%) and Milli-Q water under air. Solutions of pH 3 or 11 were prepared by adding H_2SO_4 (Wako, 95.0%) or KOH (Wako, 96.0%), respectively, to the original solution. Sulfuric acid was used instead of HCl because the latter is volatile and can possibly corrode the metal of the microscope. An electrolyte, KCl in this study, is usually added to reduce the thickness of the electric double layers on the scanned object and the scanning tip for AFM imaging. The double layers, when overlapped, produce a repulsive force on the tip, which decays monotonically with increasing tip–surface distance. The double-layer force had a negative effect in precise tracing the atomic-scale surface topography because its decay length is characterized by the Debye length, which is 1 nm in our KCl solution of pH 6.

Frequency-modulation detection of the force on the scanning tip was realized using a prototype of SPM-8100FM microscope (Shimadzu), which was enclosed in a temperature-regulated container (Mitsubishi Electric Engineering, CN-40A) maintained at 27°C. For topographic imaging of the wafer, resonance oscillation of a silicon cantilever (Nanoworld, PPP-NCHAuD) was excited mechanically with a piezo actuator. The nominal spring constant of the cantilever was 40 N/m. The resonant frequency in the imaging solutions was 130–160 kHz with a resonance quality factor of ~10. A typical spectrum of the thermally excited cantilever oscillation is shown in Fig. 2. In the imaging scans, the oscillation amplitude was regulated at a preset peak-to-peak amplitude (A) of typically 1 nm. The resonant frequency of the cantilever oscillation (f) shifts in response to the presence of a force gradient on the tip. The topography of the wafer was traced with regulation of the tip–surface distance by keeping the frequency shift (Δf) at a prefixed setpoint. The observed images were viewed and analyzed using WSxM,[23] ImageJ,[24] LabVIEW (National Instruments), and a home-made routine in Python. The typical acquisition time was 10 s per 10-nm square frame composed of 256 × 256 pixels.

Insert Fig. 2 here

FIG. 2. Typical spectrum of thermally excited cantilever oscillation in a pH-6 KCl solution. The quality factor of the resonance oscillation was deduced to be 10 by fitting the spectrum with the nominal spring constant of the cantilever.

III. SURFACE TOPOGRAPHY IN SOLUTIONS

A. Terraces and steps

The annealed TiO_2(110) wafers presented terraces and steps in the KCl solutions with different pHs. Figure 3 shows topographic images observed with positive Δf setpoints, i.e., a repulsive tip–surface force. Terraces of 100 nm or larger in width were terminated by regular-height steps. The step heights were 0.34–0.36 nm as shown in the cross-sectional images. The observed heights are consistent with the minimum step height predicted in the (110) truncation, namely 0.33 nm. The deviations can be ascribed to incomplete calibration of the *z* coordinate. The steps were nearly straight with no sign of etching in solutions of pH 3, 6, and 11. Uetsuka *et al.*[25] found 10-nm inlet-shaped steps on rutile (110) wafers immersed in neutral water or aqueous ammonia, and they ascribed the inlet-shaped steps to etching induced by the liquids. Their rutile wafers were sputtered with argon ions and vacuum-annealed, while the wafers in the present work were annealed in oxidative atmospheres. The different annealing environments led to different degrees of reduction. The annealed wafers in the present work were colorless, while the vacuum-annealed TiO_2 wafers had a blue color that depended on the temperature and annealing time.[26] The different degrees of reduction may have caused different sensitivities to the solution-induced etching. The observed stability was in agreement with the Pourbaix diagram of stoichiometric TiO_2.[27]

Insert Fig. 3 here

FIG. 3. Terraces and steps with regular height on rutile (110) wafers. Images (a)–(c) were obtained in KCl solutions with pHs of 3, 6, and 11, respectively. White scale bars of 100 nm are inserted. Cross sections along lines A–B and C–D are shown below the images. Cantilever oscillation amplitude (*A*): 1.0 nm. Frequency-shift (Δf) setpoint: (a) +176, (b) +147, and (c) +100 Hz. Acquisition time: 500 s per 400-nm square frame composed of 256 × 256 pixels.

B. Atomic-scale features

To begin with, topographic images from a pH-6 solution close to the isoelectric point were taken; here, the number of charged species adsorbed on the TiO_2 surface was minimized. Figure 4(a) presents an 8-nm square image smoothed with a moving average of 3 × 3 pixels. The raw image prior to the smoothing is available in Fig. S2. The imaged wafer was prepared just thorough annealing at 1000°C in the sapphire tube by skipping second-stage annealing in the quartz tube. The bright (dark) color shows protrusions (depressions) on the surface. The most apparent feature was the bright ridges parallel to the [001] axis with dark trenches in between. The A–B cross section was determined perpendicular to the ridge axis and is shown in Fig. 4(b). The ridge-to-ridge distance was controlled at 0.73 nm, and the length was deduced from the autocorrelation as described in the following paragraphs. The peak-to-peak amplitude of the topographic corrugation was 0.1 nm.

Corrugations along the ridge axis were also recognized. The C–D cross section exhibited periodic corrugations with a repetition length of 0.27 nm along the axis. The topographic amplitude was as small as 0.03 nm in the C–D cross section and was even smaller on other ridges.

Because the repetition lengths are essential for interpreting the visualized species, the autocorrelation of the raw image was calculated. Autocorrelation provides a method for deducing statistically the short-range order of imaged objects, which are the atomic-size protrusions here. On the TiO_2(110) wafers placed in a vacuum, the short-range order of Cl atoms,[28] formate anions,[29] and N3 dye molecules[30] was analyzed quantitatively via autocorrelation. Fourier transformation is a convenient method for detecting long-range order in the imaged samples, but unfortunately our topographic images were affected by drift, as is frequently the case with imaging in liquid. Hence, we used autocorrelation to recognize the short-range order in the topographic image, which should reflect long-range ordering in an ideal image free from drift artifacts.

The autocorrelation $F(x, y)$ was calculated as a function of the correlation vector (x, y) as

$$F(x,y) = \sum_{X,Y} \{H(X,Y) \cdot H(X+x, Y+y)\},$$

where $H(X, Y)$ presents the topographic height in the raw image, prior to moving average, at the lateral coordinates of (X, Y). In the summation, (X, Y) runs over the pixels in the raw image.[31] The autocorrelation reflects the relative location of two atomic-scale protrusions. $F(x, y)$ has its maximum at the origin and is normalized to be unity representing the position of the first protrusion. The correlation increases at (x, y) where the occupation probability of a second protrusion is high.

The 3-nm square autocorrelation was thereby calculated and shown beside the raw image in Fig. 4(a). The ridges recognized in the raw image produced bright grids parallel to the [001] axis in the autocorrelation, while the corrugations along the ridges were missing on visual inspection. The autocorrelation was investigated further by taking cross sections along lines involving the origin, as shown in Fig. 4(c). The cross section perpendicular to the ridge axis yielded a ridge-to-ridge distance of 0.73 nm. The other cross section, which was parallel to the ridge axis, exhibited small but finite corrugations superposed on a feature decaying monotonously with the lateral distance from the origin. The corrugations were periodic with a repetition length of 0.27 nm. The corrugations in the A–B and C–D cross sections fitted well with the repetition lengths determined from the autocorrelation. Hence, it could be concluded that the autocorrelation provided the correct average length for the short-range order from the raw image. Atomic-scale protrusions were located on meshes of 0.73 nm in the $[1\bar{1}0]$ direction by 0.27 nm in the [001] axis. To verify reproducibility, another image observed on the same wafer with a different cantilever was analyzed similarly; the results showed compatible meshes of 0.73 nm by 0.28 nm, as shown in Fig. S3.

The repetition lengths observed in Fig. 4, namely 0.73 and 0.27 nm, were in agreement with those of the (1×1) unit cell, namely 0.65 and 0.30 nm,[32] which had a precision of 13% or better. Hence, the atomic-scale protrusions were assigned to the bridging oxygen anions. The anions were located on the (1×1) meshes and protruded from the surface plane to the solution when the (110) surface had the topography illustrated in Fig. 1. The corrugation amplitudes of 0.1 and 0.03 nm determined from the A–B and C–D cross sections, respectively, did not conflict with the assignment of the protrusions to the bridging oxygen anions.

For comparison, Serrano *et al.*[33] conducted topographic imaging of TiO_2(110) wafers prepared in vacuum and submerged in water using scanning tunneling microscopy (STM). They reported ridges and trenches parallel to the [001] axis with a repetition length of 0.70 nm, which is in agreement with the results obtained in the present study. Furthermore, they observed two-fold periodicity along the axis and attributed this to hydrogen-bonded water dimers trapped on the five-fold coordinated Ti cations at the bottom of the trenches; by contrast, a one-fold periodicity was observed in the present work. One explanation for the contrasting results could be the different imaging techniques used, namely STM versus AFM in the present study. While the water dimers hypothesized in the STM study may be trapped weakly in the trenches, in the present study the AFM tip may have pushed the dimers aside; further work should be carried out to confirm this hypothesis. The mechanical

force on the AFM tip was ~0.1 nN, while the force on the STM tip was not determined. The imaging liquid was the KCl solution exposed to air in the present study, while pure water degassed by bubbling with argon gas was used in the STM study.

Two-fold periodicity along the [001] axis has been reported in a number of STM studies on vacuum-prepared TiO_2(110) wafers exposed to liquid water or water vapor followed by scanning in a vacuum. The observed two-fold periodicity was attributed to OH,[34] bicarbonate,[35] or OOH species[36] chemisorbed on the surface. Balajka *et al.*[37] found that a (110) wafer exposed to purified liquid water exhibited one-fold periodicity; they pointed out that chemisorbed formate and/or acetate anions may have produced the two-fold periodicity observed on wafers that were exposed to water and then dried. These previous results on dried wafers do not necessarily reproduce the observation conditions in liquid water. Because water is a good solvent, the presence or absence of the chemical species that were proposed to form two-fold periodicity would be sensitive to the environment during scanning.

A–B and C–D cross sections were at an angle of 78º in Fig. 4(a). The ridge-to-ridge distance in A–B cross section is thus to be corrected by -2% because of the angle finitely deviated from 90º. The required correction was 0.1 nm in ridge-to-ridge distance being less than precision in our topographic imaging affected by drifts.

Insert Fig. 4 here

FIG. 4. Atomic-scale topography of rutile (110) wafer in pH-6 KCl solution. An 8-nm square raw topographic image with a moving average filter is shown in (a) with A–B and C–D cross sections in (b). The 3-nm square autocorrelation of the raw image is shown in the small image at the side. The normalized autocorrelation is presented in (c) as a function of lateral coordinates parallel to the $[1\bar{1}0]$ and [001] directions. A: 0.8 nm. Δf setpoint: +288 Hz.

Next, the topography observed in a basic solution of pH 11 is analyzed. Figure 5 shows an image with a moving average filter and the autocorrelation together with their cross sections. For the basic solution, it was more difficult to recognize ridges and trenches parallel to the [001] axis by visual inspection of the filtered image; atomic-size swellings were located in a less ordered manner than the observed protrusions in the pH-6 solution. Corrugations in the A–B cross section were less periodic, and they fitted the 0.68-nm grids. The

autocorrelation demonstrated that the swellings appeared in line along the [001] axis with a line-to-line distance of 0.63 nm. The less-ordered distribution of swellings resulted in the determination of slightly different repetition lengths of 0.68 nm for the A–B cross section and 0.63 nm by autocorrelation. The length with the autocorrelation represented the short-range order averaged over the raw image. Another image observed on the same wafer with the same cantilever presented a repetition length of 0.75 nm for the autocorrelation, as shown in Fig. S5. The observed repetition lengths ranging between 0.63–0.75 nm indicated one-fold periodicity along the [1−10] direction.

A two-fold periodicity was observed along the [001] axis. In the C–D cross section, swellings were observed with a repetition length of 0.45 nm. The amplitudes of the corrugations were 0.05 nm, which was comparable with or larger than the corrugation amplitude determined in the C–D cross section for the pH-6 solution. The autocorrelation had the same repetition length along the axis. On the surface shown in Fig. S5, the repetition length along the axis was 0.60 nm.

Signal-to-background ratio was unfortunately low in the normalized autocorrelation curve parallel to the [001] axis. Periodic corrugations were clearer in C–D cross section of the corresponding images than those in the normalized autocorrelation curve. The authors superposed the grids of 0.45 nm on the autocorrelation curves for eye guide. Presenting autocorrelation results are necessary for showing short-range order averaged over the 8-nm square images, while individual cross sections representing local short-range order.

The observed repetition length of 0.45–0.60 nm is twice that of the unit cell length along the axis. Swellings lined in the two-fold periodicity along the [001] axis should produce a superstructure with either p(2×1) or c(2×2) symmetry. From visual inspection of the 3-nm square autocorrelations in Figs. 5 and S5, p(2×1) symmetry with two neighboring lines in phase can be determined. Therefore, short-range p(2×1) order can be concluded for the swelling distribution.

The cause of the two-fold periodicity is considered. The basic solution included KOH (10^{-4} mol/L) in addition to the KCl electrolyte (0.1 mol/L). The OH^- species in the solution should be responsible for the modified periodicity. The equilibrated deprotonation of Ti-OH_2 shifts to produce Ti-OH^- on the five-fold coordinated Ti cations. In addition, direct adsorption of the OH^- species from solution is also possible. When the OH^- species were chemisorbed tightly enough to thrust the AFM tip backward, they appear as swellings in the topographic images. The Ti-OH^- bond was perpendicular to the surface plane with a bond length of 0.20 nm according to

an X-ray crystal truncation rod study conducted in a RbCl solution of pH 12.[32] The same study showed that the bridging oxygen anions were lifted by 0.14 nm from the plane containing Ti cations. Hence, the oxygen atom in the upright adsorbed OH^- protruded by 0.06 nm over the plane defined by the bridging oxygen anions. For the pH-11 solution, two-fold periodicity appears when further assuming that the coverage of the OH^- species was 50% relative to the five-fold coordinated Ti cations, as observed in Fig. 5. The negatively charged species should be distributed evenly in each trench to reduce electrostatic repulsion. Therefore, it can be hypothesized that the OH^- species chemisorbed on the five-fold coordinated Ti cations caused the swellings visualized in Figs. 5 and S5.

Balajka *et al.*[37] proposed that carboxylic acids, particularly formic acid and acetic acid, contaminating in imaging solution are dissociatively adsorbed on TiO_2(110) and produced two-fold symmetry along the [001] axis. The possible concentration of the contaminating compounds should be far less than their solubility in the KCl solution. Hence, the concentration of contaminating acids, if any, cannot be sensitive to the pH of the KCl solution. Acid adsorption enhanced in our basic solution to form two-fold symmetry is less possible.

Insert Fig. 5 here

FIG. 5. Atomic-scale topography of rutile (110) wafer in pH-11 KCl solution. An 8-nm square, moving-average filtered image is shown in (a) with A–B and C–D cross sections in (b). The 3-nm square autocorrelation of the raw image presents the small gray-scale image at the side. The normalized autocorrelation is presented in (c) as a function of lateral coordinates parallel to the $[1\bar{1}0]$ and [001] directions. *A*: 0.7 nm. Δf setpoint: +137 Hz. The raw topographic image prior to the smoothing is shown in Fig. S4.

Finally, the topography in the acidic solution with pH 3 was examined. The results shown in Figs. 6 and S7 are qualitatively similar to those observed in the neutral pH-6 solution. Ridges and trenches parallel to the [001] axis were present with a repetition length of 0.60 nm. It was not easy to identify periodicity along the axis. Repetition lengths of 0.30 (Fig. 6) and 0.29 nm (Fig. S7) along the ridge axis can be determined. The observed repetition lengths suggested atomic-scale protrusions on (1×1) meshes. Hence, the protrusions were assigned to the bridging oxygen anions, as in the neutral solution.

Because the solution was more acidic than the isoelectric point, the bridging oxygen anions accommodated the protons either fully or partially. In principle, the topographic height of a bridging anion should be sensitive to the presence or absence of the adsorbed proton. However, the proton-induced difference in topography may not have been sufficient given the resolution of the topographic imaging. There were no indications of HSO_4^- or SO_4^{2-} anions adsorbed on the TiO_2 surface.

Insert Fig. 6 here

FIG. 6. Atomic-scale topography of rutile (110) wafer in pH-3 KCl solution. An 8-nm square, moving-average filtered image is shown in (a) with A–B and C–D cross sections in (b). The 3-nm square autocorrelation of the raw image presents the small gray-scale image at the side. The normalized autocorrelation is presented in (c) as a function of lateral coordinates parallel to the $[1\bar{1}0]$ and [001] directions. A: 1.0 nm. Δf setpoint: +321 Hz. The raw topographic image prior to the smoothing is shown in Fig. S6.

4. CONCLUSION

In this work, the atomic-scale topography of (110)-oriented rutile TiO_2 wafers annealed in an oxidative atmosphere was investigated; they presented crystalline terraces in aqueous KCl solutions with pH 3, 6, and 11 with no sign of solution-induced etching. The frequency-modulation detection of the tip–surface force enabled topographic imaging of the terraces with atomic-scale resolution. Atomic-size protrusions were recognized in solutions with pH 6, while they were observed less clearly in a solution of pH 3. The protrusions were located on the (1×1) meshes of the (110) surface and assigned to bridging oxygen anions protruding from the surface plane to the solution. In a basic solution of pH 11, atomic-size swellings were observed, which were hypothesized to be Ti-OH^- on the five-fold coordinated Ti cations covering the surface to form a p(2×1) superstructure. This work shows the feasibility of FM-AFM for atomic-scale imaging of metal-oxide surfaces submerged in water.

SUPPLEMENTARY MATERIAL

See supplementary material for an assessment of the reproducibility in the topographic imaging.

ACKNOWLEDGMENTS

This work was supported by JSPS KAKENHI grant number JP18K19058.

[1] U. Diebold, "The surface science of titanium dioxide," Surf. Sci. Rept. **48**, 53–230 (2003).

[2] U. Diebold, "Perspective: A controversial benchmark system for water-oxide interfaces: $H_2O/TiO_2(110)$," J. Chem. Phys. **147**, 040901 (2017).

[3] F. J. Giessibl, "Atomic resolution of the silicon (111)-(7x7) surface by atomic force microscopy," Science **267**, 68–71 (1995).

[4] S. Kitamura, and M. Iwatsuki, "Observation of 7×7 reconstructed structure on the silicon (111) surface using ultrahigh vacuum noncontact atomic force microscopy," Jpn. J. Appl. Phys. **34**, L145–L148 (1995).

[5] Y. Sugawara, M. Ohta, H. Ueyama, and S. Morita, "Defect motion on an InP (110) surface observed with noncontact atomic force microscopy," Science **270**, 1646–1648 (1995).

[6] A. Sasahara, S. Kitamura, H. Uetsuka, and H. Onishi, "Oxygen-atom vacancies imaged by a noncontact atomic force microscope operated in an atmospheric pressure of N_2 gas," J. Phys. Chem. B **108**, 15735–15737 (2004).

[7] T. Fukuma, M. Kimura, K. Kobayashi, K. Matsushige, and H. Yamada, "Development of low noise cantilever deflection sensor for multienvironment frequency-modulation atomic force microscopy," Rev. Sci. Instrum. **76**, 053704 (2005).

[8] T. Fukuma, K. Kobayashi, K. Matsushige, and H. Yamada, "True molecular resolution in liquid by frequency-modulation atomic force microscopy," Appl. Phys. Lett. **86**, 193108 (2005).

[9] S.-H. Loh, and S. Jarvis, "Visualization of ion distribution at the mica–electrolyte interface," Langmuir **26**, 9176–9178 (2010).

[10] T. Hiasa, K. Kimura, H. Onishi, M. Ohta, K. Watanabe, R. Kokawa, N. Oyabu, K. Kobayashi, and H. Yamada, "Aqueous Solution Structure over α-$Al_2O_3(01\bar{1}2)$ Probed by Frequency-Modulation Atomic Force Microscopy," J. Phys. Chem. C **114**, 21423–21426 (2010).

[11] Y. Araki, H. Satoh, M. Okumura, and H. Onishi, "Localization of cesium on montmorillonite surface investigated by frequency modulation atomic force microscopy," Surf. Sci. **665**, 32–36 (2017).

[12] K. Umeda, L. Zivanovic, K. Kobayashi, J. Ritala, H. Kominami, P. Spijker, A. S. Foster, and H. Yamada, "Atomic-resolution three-dimensional hydration structures on a heterogeneously charged surface," Nat. Commun. **8**, 2111 (2017).

[13] K. Umeda, K. Kobayashi, T. Minato, and H. Yamada, "Atomic-scale 3D local hydration structures influenced by water-restricting dimensions," Langmuir **34**, 9114–9121 (2018).

[14] S. Kawasaki, E. Holmström, R. Takahashi, P. Spijker, A. S. Foster, H. Onishi, and M. Lippmaa, "Intrinsic superhydrophilicity of titania-terminated surfaces," J. Phys. Chem. C **121**, 2268–2275 (2017).

[15] H. Asakawa, E. Holmström, A.S. Foster, S. Kamimura, T. Ohno, and T. Fukuma, "Direct Imaging of atomic-scale surface structures of brookite TiO_2 nanoparticles by frequency modulation atomic force microscopy in liquid," J. Phys. Chem. C **122**, 24085–24093 (2018).

[16] A. Sasahara, and M. Tomitori, "Frequency modulation atomic force microscope observation of TiO_2(110) surfaces in water," J. Vac. Sci. Technol. B **28**, C4C5–C4C10 (2010).

[17] K. Fukui, H. Onishi, and Y. Iwasawa, "Atom-resolved image of the TiO_2 (110) surface by noncontact atomic force microscopy," Phys. Rev. Lett. 79, 4202–4205 (1997).

[18] R. Bechstein, C. González, J. Schütte, P. Jelínek, R. Pérez, and A. Kühnle, "'All-inclusive' imaging of the rutile TiO_2(110) surface using NC-AFM," Nanotechnology, **20**, 505703 (2009).

[19] J. P. Fitts, M. L. Machesky, D. J. Wesolowski, X. Shang, J. D. Kubicki, G. W. Flynn, T. F. Heinz, and K. B. Eisenthal, "Second-harmonic generation and theoretical studies of protonation at the water/α-TiO_2(110) interface," Chem. Phys. Lett. **411**, 399–403(2005).

[20] J. Cheng, and M. Sprik, "Acidity of the aqueous rutile TiO_2 (110) surface from density functional theory based molecular dynamics," J. Chem. Theory Comput. **6**, 880–889 (2010).

[21] J. W. Bullard, and M. J. Cima, "Orientation dependence of the isoelectric point of TiO_2 (rutile) surfaces," Langmuir **22**, 10264–10271 (2006).

[22] A. Sasahara, T. Murakami, and M. Tomitori, "Nanoscale characterization of TiO_2 (110) annealed in air," Appl. Surf. Sci. **428**, 1000–1005 (2018).

[23] I. Horcas, R. Fernández, J.M. Gomez-Rodriguez, and A.M. Baro, "WSXM: a software for scanning probe microscopy and a tool for nanotechnology," Rev. Sci. Instrum. **78**, 013705 (2007).

[24] C. A. Schneider, W. S. Rasband, and K. W. Eliceiri, "NIH Image to ImageJ: 25 years of image analysis," Nat. Methods **9**, 671–675 (2012).

[25] H. Uetsuka, A. Sasahara, and H. Onishi, "Topography of the rutile TiO_2 (110) surface exposed to water and organic solvents," Langmuir, **20**, 4782–4783 (2004).

[26] M. Li, W. Hebenstreit, U. Diebold, A.M. Tyryshkin, M.K. Bowman, G.G. Dunham, and M.A. Henderson, "The Influence of the Bulk Reduction State on the Surface Structure and Morphology of Rutile TiO_2(110) Single Crystals," J. Phys. Chem. B **104**, 4944–4950 (2000).

[27] J. W. Schultze, M. M. Lohrengel, "Stability, reactivity and breakdown of passive films. Problems of recent and future research," Electrochim. Acta **45**, 2499–2513 (2000).

[28] U. Diebold, W. Hebenstreit, G. Leonardelli, M. Schmid, and P. Varga. "High transient mobility of chlorine on TiO_2(110): evidence for "cannon-ball" trajectories of hot adsorbates," Phys. Rev. Lett. **81**, 405–408 (1998).

[29] H. Onishi, K. Fukui, and Y. Iwasawa, "Space-correlation analysis of formate ions adsorbed on TiO_2(110)," Jpn. J. Appl. Phys. **38**, 3830–3832 (1999).

[30] M. Ikeda, N. Koide, L. Han, C. Pang, A. Sasahara, and H. Onishi, "Lateral distribution of N3 dye molecules on TiO_2(110) surface," J. Photochem. Photobio. A **202**, 185–190 (2009).

[31] $F(x, y)$ should be symmetric with respect to the origin by definition. The authors practically restricted the summation range of (X, Y) not to place $(X+x, Y+y)$ out of the raw image. The autocorrelation summed under the restriction slightly deviated from the inversion symmetry.

[32] Z. Zhang, P. Fenter, N. C. Sturchio, M. J. Bedzyk, M. L. Machesky, and D. J. Wesolowski, "Structure of rutile TiO_2(110) in water and 1 molal Rb^+ at pH 12: inter-relationship among surface charge, interfacial hydration structure, and substrate structural displacements," Surf. Sci. **601**, 1129–1143 (2007).

[33] G. Serrano, B. Bonanni, M. Di Giovannantonio, T. Kosmala, M. Schmid, U. Diebold, A. Di Carlo, J. Cheng, J. VandeVondele, K. Wandelt, and C. Goletti, "Molecular ordering at the interface between liquid water and rutile TiO_2(110)," Adv. Mater. Interfaces **2**, 1500246 (2015).

[34] H. Hussain, G. Tocci, T. Woolcot, X. Torrelles, C. L. Pang, D. S Humphrey, C. M. Yim, D. C. Grinter, G. Cabailh, O. Bikondoa, R. Lindsay, J. Zegenhagen, A. Michaelides, and G. Thornton, "Structure of a model TiO_2 photocatalytic interface," Nat. Mater. **16**, 461–466 (2017).

[35] A. Song, E. S. Skibinski, W. J. I. DeBenedetti, A. G. Ortoll-Bloch, and M. A. Hines, "Nanoscale solvation leads to spontaneous formation of a bicarbonate monolayer on rutile (110) under ambient conditions: Implications for CO_2 photoreduction," J. Phys. Chem. C **120**, 9326–9333 (2016).

[36] A. Sasahara, and M. Tomitori, "An atomic-scale study of TiO_2(110) surfaces exposed to humid environments," J. Phys. Chem. C **120**, 21427–21435 (2016).

[37] J. Balajka, M. A. Hines, W. J. I. DeBenedetti, M. Komora, J. Pavelec, M. Schmid, and U. Diebold, "High-affinity adsorption leads to molecularly ordered interfaces on TiO_2 in air and solution," Science **361**, 786–789 (2018).

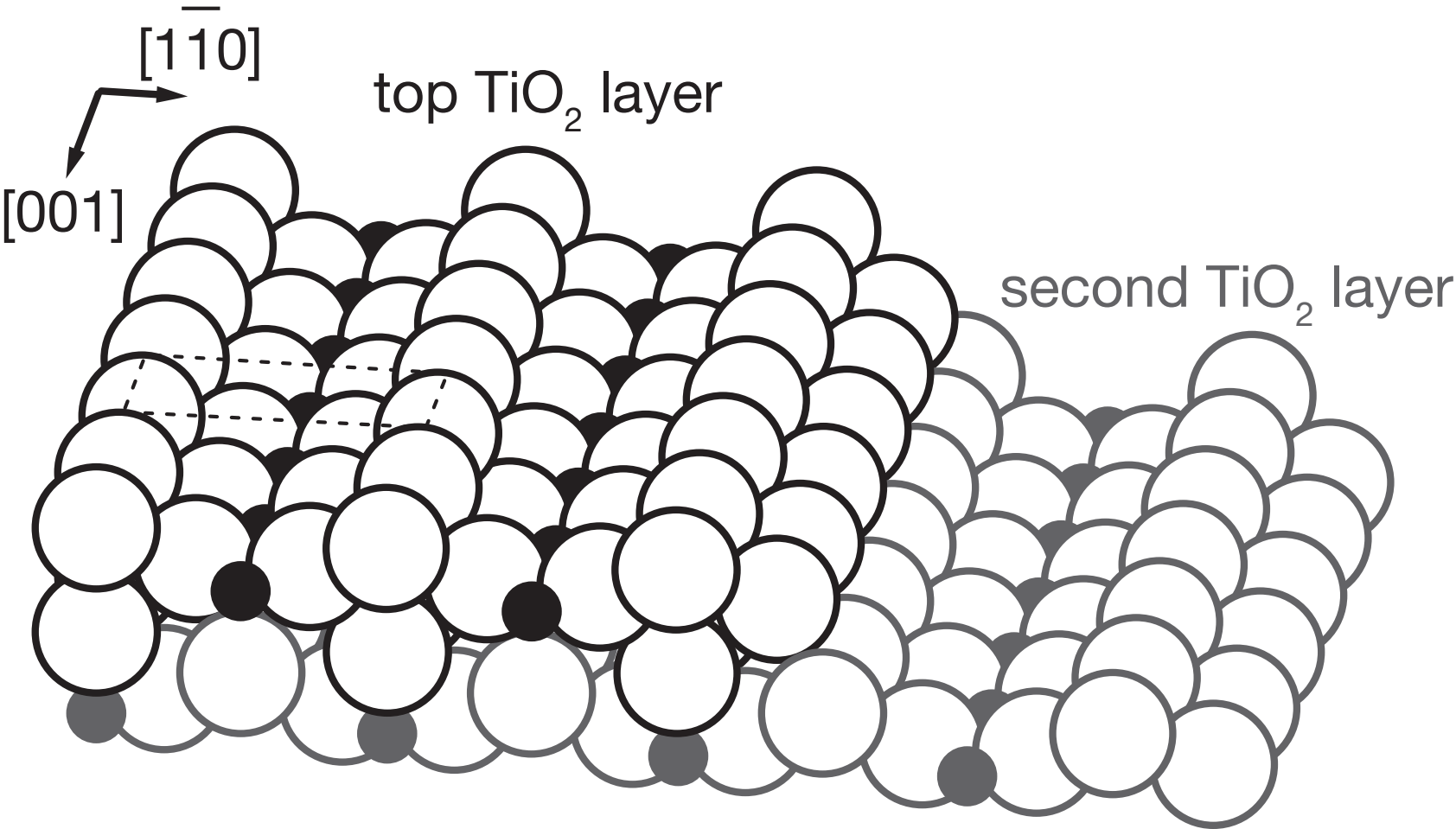
[1$\bar{1}$0]
[001]
top TiO_2 layer
second TiO_2 layer

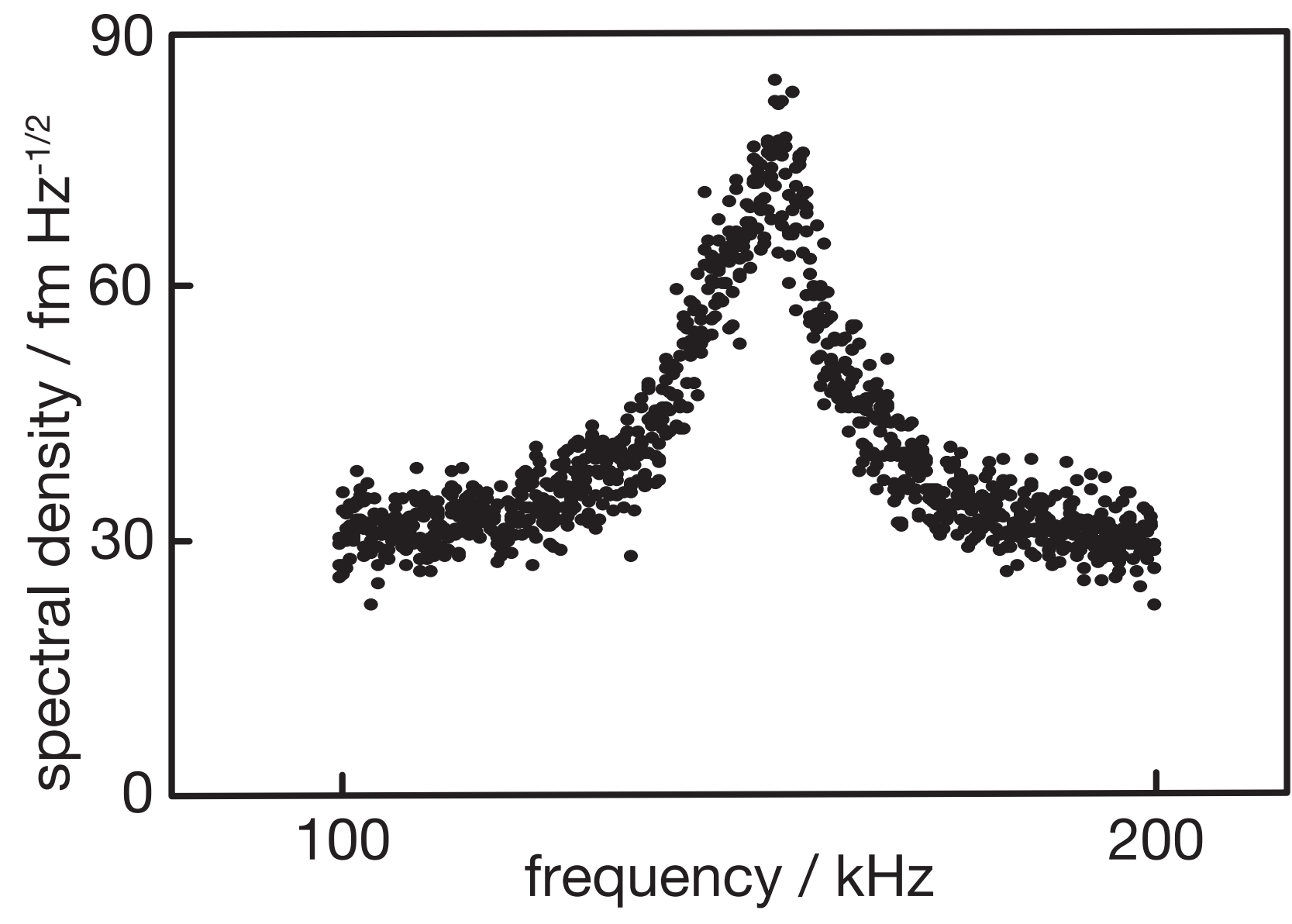
90
60
30
0
spectral density / fm Hz-1/2
100
200
frequency / kHz

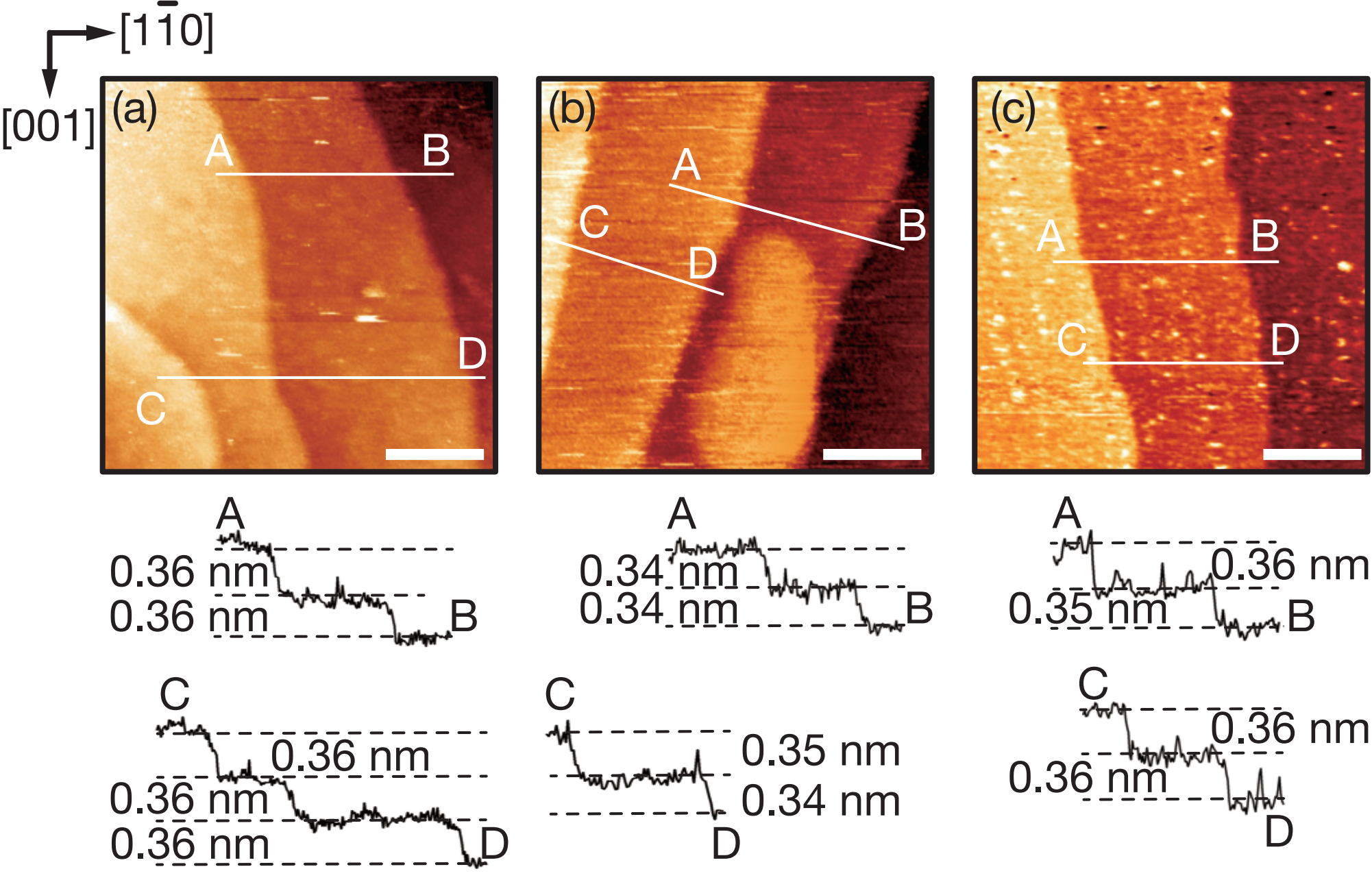
[1$\bar{1}$0]
[001]
(a)
A
B
C
D
(b)
A
B
C
D
(c)
A
B
C
D
A
0.36 nm
0.36 nm
B
A
0.34 nm
0.34 nm
B
A
0.35 nm
0.36 nm
B
C
0.36 nm
0.36 nm
0.36 nm
D
C
0.35 nm
0.34 nm
D
C
0.36 nm
0.36 nm
D

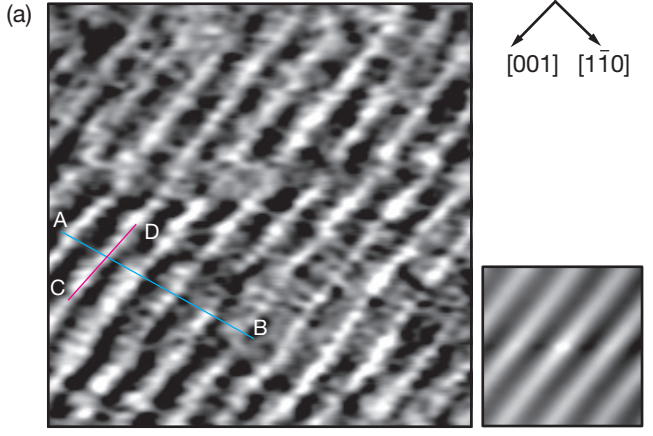
(a)
[001]
[1$\bar{1}$0]
A
D
C
B

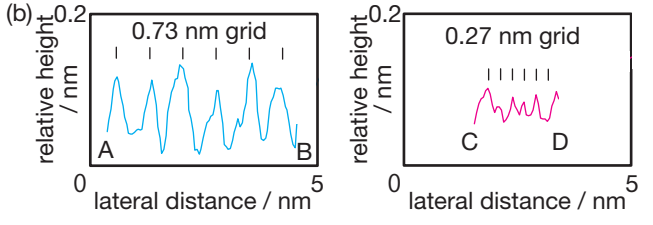
(b)
relative height / nm
0.2
0.73 nm grid
A
B
0
5
lateral distance / nm
relative height / nm
0.2
0.27 nm grid
C
D
0
5
lateral distance / nm

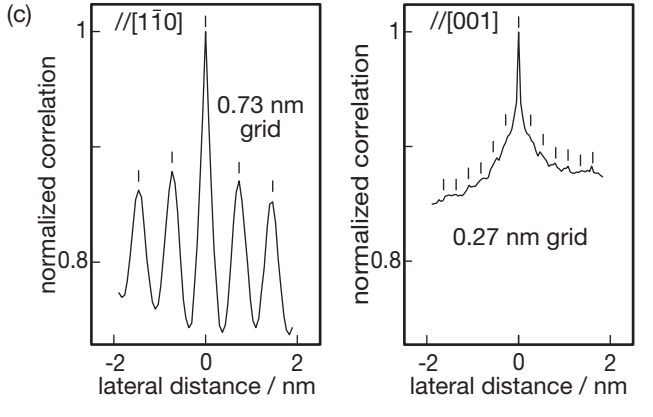
(c)
normalized correlation
1
0.8
//[1$\bar{1}$0]
0.73 nm grid
-2
0
2
lateral distance / nm
normalized correlation
1
0.8
//[001]
0.27 nm grid
-2
0
2
lateral distance / nm

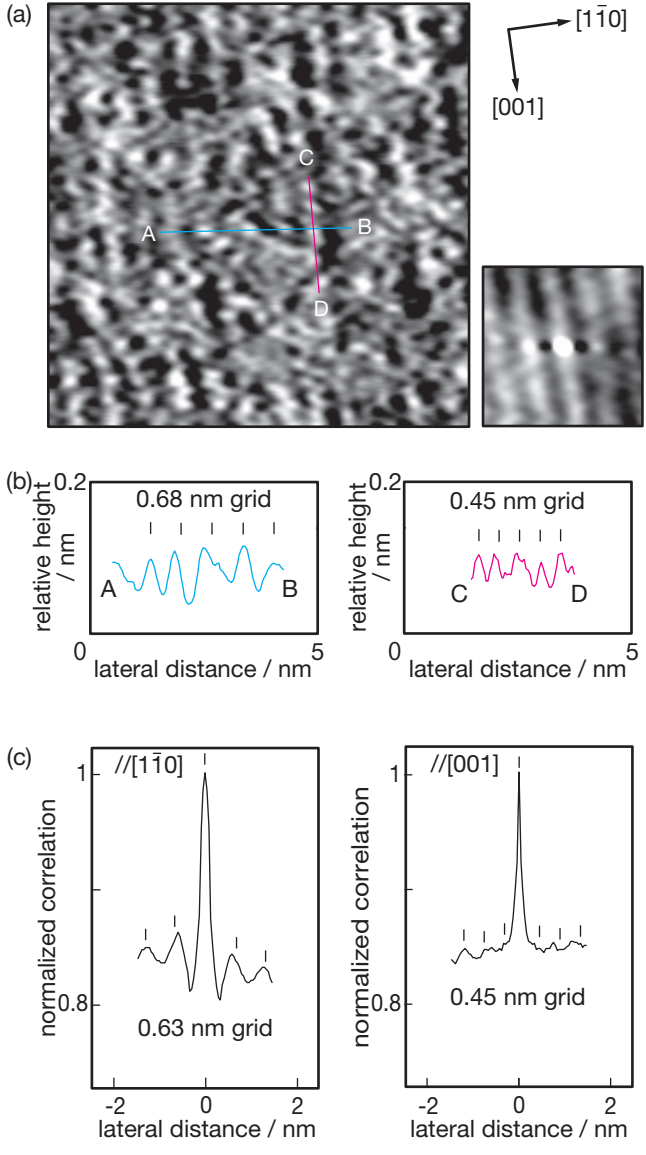
(a)
[1$\bar{1}$0]
[001]
A
B
C
D
(b)
0.68 nm grid
relative height / nm
0.2
A
B
0
5
lateral distance / nm
0.45 nm grid
relative height / nm
0.2
C
D
0
5
lateral distance / nm
(c)
//[1$\bar{1}$0]
1
0.8
normalized correlation
0.63 nm grid
-2
0
2
lateral distance / nm
//[001]
1
0.8
normalized correlation
0.45 nm grid
-2
0
2
lateral distance / nm

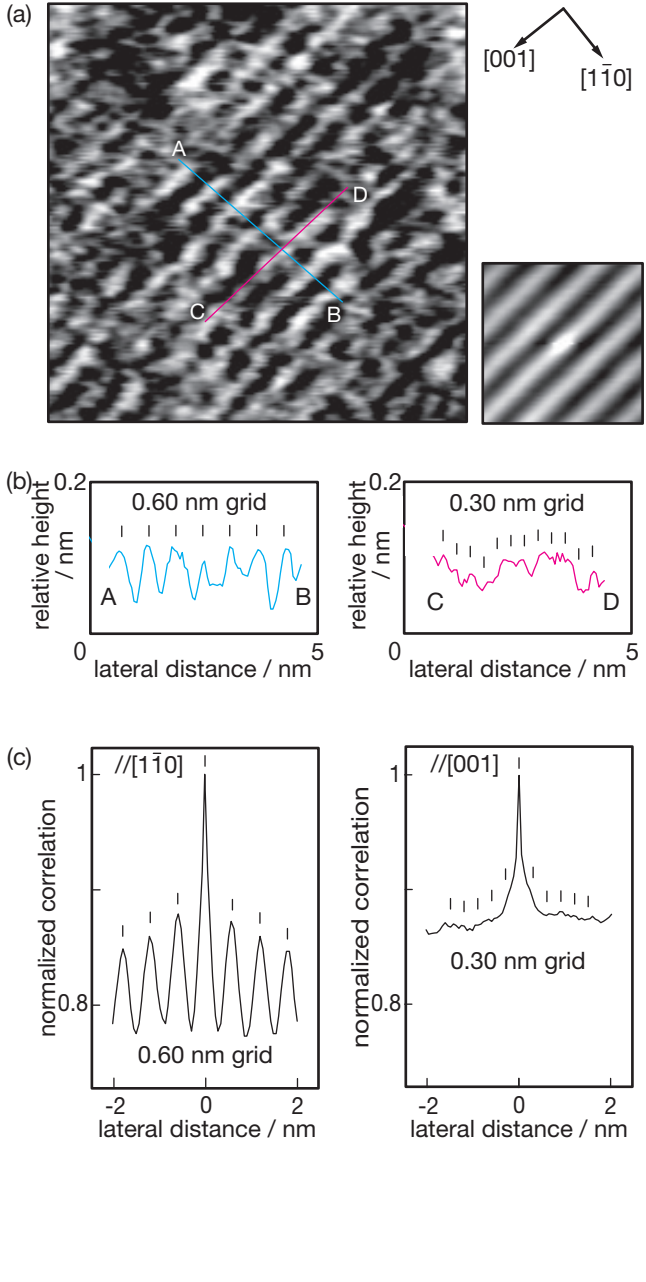
(a)
[001]
[1$\bar{1}$0]
A
B
C
D
(b)
relative height / nm
0.2
0
0.60 nm grid
A
B
5
lateral distance / nm
0.30 nm grid
C
D
(c)
normalized correlation
1
0.8
//[1$\bar{1}$0]
0.60 nm grid
-2
0
2
lateral distance / nm
//[001]
0.30 nm grid